Fast Beamforming with Circular Receiving Arrays

Abstract: The Fast Fourier Transform (FFT) can be applied to circular arrays receiving wideband sonar radiation. As with conventional beamforming, the FFT serves in the first stage to divide the spectrum into narrow frequency bands. Then the array element responses of each band are analyzed in a second stage of FFTs for the Fourier components (modes) of the array excitation function for the respective band. Application of weights of the mode responses, to simulate the radiation efficiency of the modes for any given element radiation pattern and to control the array pattern, yields the Fourier components of the beam pattern. To integrate these Fourier components, inverse FFTs follow which yield as many beam pattern samples as there are array elements.

Contents

Introduction	398
Modal representation of the array excitation function	399
Radiation coefficient of a mode	400
Pattern synthesis from spatial frequency components and array design constraints	402
The beamforming network and its theory	403
Cophasal beam excitation function and pattern of a circular array	405
Computer simulation of the fast beamforming	407

Introduction

Circular arrays have been studied extensively because they offer several unique features:

- Beam shapes in the plane of the array, the azimuth plane, are essentially independent of the steering angle [1].
- The beam direction is independent of the signal frequency even when phase shifters, rather than delay lines, are employed in the feed lines of the elements [2].
- · Radiation that is omnidirectional in azimuth can be achieved with beams directional in elevation, e.g., conical beams [3, 4].

If the excitation of each array element is first determined for a desired beam shape, the conventional circuit then consists of phase shifters and attenuators inserted in all feed lines, save one for each beam, and a combiner for all the line outputs [5]. Because each component serves only one directive beam in azimuth and the number of contiguous beams equals the number of array elements, N, the number of beamforming components increases as N(N-1). Geometrically simple arrays can, however, lead to beamforming networks with fewer components. For example, the beam cophasal excitation of a linear array requires phase shifts in the feed lines that vary by uniform steps across the array. This led Butler and Lowe [6] to design, for electromagnetic arrays, a matrix network of interconnected feed lines in which phase shifters serve multiple beams simultaneously. Besides simple phase shifters, hybrids are used which shift phases and also add. Thus the numbers of phase shifters and hybrids are only $(N/2) \log_{9} N$ and $(N/2)(\log_2 N - 1)$, respectively. The analog techniques are, of course, instantaneous beamformers and the advantage of the Butler matrix lies in the saving of components. Because the excitation function of a linear radiator and the corresponding farfield pattern are related by the Fourier transform, the Butler matrix generates samples of the Fourier transform of the array excitation.

Computationally, the phase shift and attenuation of a signal is a complex multiplication. If the signal can be sampled at a sufficiently low rate, as is the case with sonar signals, digital multiplications and additions can be performed in real time. Hence the number of multiplications would be equal to the number of phase shifters if the flow of computations would follow the analog process. Because digital multiplications take time and are performed sequentially, computations according to the Butler matrix can be completed in a much shorter time than computations according to the conventional circuit.

Investigators of sonar arrays, however, arrived independently at a fast beamforming (FBF) process for linear receiving arrays by introducing the Fast Fourier Transform (FFT) [7], only to realize afterwards that the FBF was the digital equivalent of the Butler matrix.

Earlier investigators of the circular array applied the conventional circuit for beamforming [8-10]. Later it was realized that the Butler matrix could also be introduced to the beam forming of circular arrays [11, 12] because any arbitrary excitation of a circular line aperture can be expressed by a spatial Fourier series [13-15], and each term constitutes an excitation function, referred to as a mode, whose phase changes by uniform steps from element to element as in the beam cophasal excitation of a linear array. It was also recognized that a one-to-one relationship existed between the spatial frequency terms of the excitation function and those of the farfield pattern [1]. Furthermore, to generate the pattern or beam response from the modes of the farfield pattern would require an inverse Fourier transform. The FFT, therefore, offers advantages in the digital beam forming process for circular arrays because it can serve sequentially as a spectral analyzer of broadband signals, as a mode former, and as a beam former. The object of this paper is to present the theory and implementation of fast beamforming with circular receiving arrays.

Modal representation of the array excitation function

An arbitrary excitation function \overline{E}_s of a circular array of M equally spaced elements can be treated as a sampled continuous periodical complex variable \overline{E} [16], so that

$$\overline{E}_{s}(\alpha_{r}) = s(\alpha_{r}) \ \overline{E}(\alpha_{r}), \tag{1}$$

where the sampling function

$$s(\alpha_r) = \delta\{\sin[(M/2) (\alpha_r - \alpha_g)]\}. \tag{2}$$

As illustrated in Fig. 1, the array is disposed on a circle of radius R in the x-y plane and concentric with the z axis. Angle α_r relates to an arbitrary position on the circle and α_e is the position of the zero-th array element. A field point is at the distance r, azimuth α , and elevation ϵ from a point on the circle, and r_0 is the distance from the center of the circle.

We are interested in the spatial frequency or mode spectrum of the excitation function. Ideally, the radiation pattern is exclusively determined by \overline{E} , but the substitution of an array for the continuous ring radiator is dictated by engineering constraints leading to pattern perturbations which must be controlled. Since \overline{E} can be expressed by its own mode spectrum, Eq. (1) can be written as

$$\overline{E}_{s}(\alpha_{r}) = s(\alpha_{r}) \sum_{q=-\infty}^{\infty} \overline{E}_{q}(\alpha_{r}) = \sum_{q=-\infty}^{\infty} s(\alpha_{r}) \overline{C}_{q} \exp[iq\alpha_{r}]$$

$$= \sum_{q=-\infty}^{\infty} \overline{E}_{qs}(\alpha_{r}). \tag{3}$$

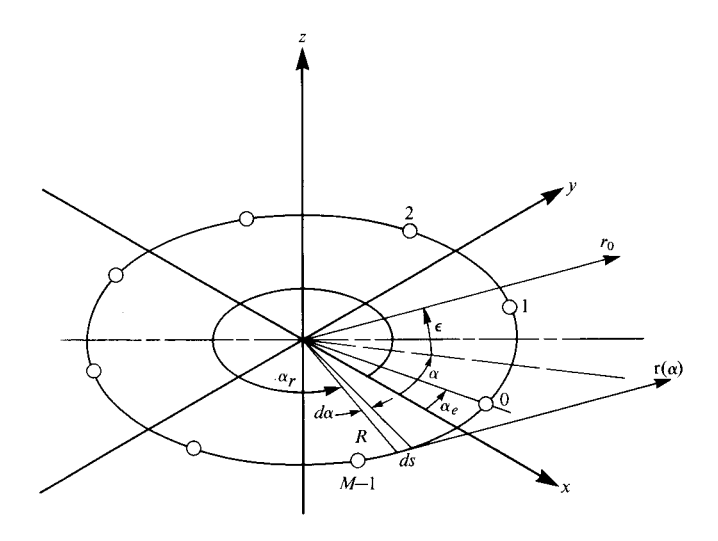


Figure 1 Coordinate system of the circular array of equally spaced elements used in deriving the spatial frequency of the excitation function.

Hence we may first derive the mode spectrum of a sampled modal excitation function $\overline{E}_{ac}(\alpha_r) \equiv \overline{E}_{ac}$,

$$\begin{split} \overline{E}_{qs} &= \delta \bigg\{ \frac{2}{M} \sin \bigg[\frac{M}{2} \; (\alpha_r - \alpha_e) \; \bigg] \bigg\} \\ &\times \cos \bigg[\frac{M}{2} \; (\alpha_r - \alpha_e) \; \bigg] \; \overline{C}_q \; \exp[jq\alpha_r] \,, \end{split} \tag{4} \end{split}$$

which can be expressed by

$$\overline{E}_{qs} = \sum_{l=-\infty}^{\infty} \overline{C}_{ql} \exp[jl\alpha_r], \tag{5}$$

where $\overline{C_{al}}$ is defined as

$$\overline{C}_{ql} = \frac{1}{2\pi} \int_{0}^{2\pi} \overline{E}_{qs} \exp[-jl\alpha_r] d\alpha_r.$$
 (6)

Now we substitute Eq. (4) into Eq. (6) and solve the integral

$$\overline{C}_{ql} = \frac{\overline{C}_q}{2\pi} \int_0^{2\pi} \delta \left\{ \frac{2}{M} \sin \left[\frac{M}{2} (\alpha_r - \alpha_e) \right] \right\} \\
\times \cos \left[\frac{M}{2} (\alpha_r - \alpha_e) \right] \exp[j(q - l)\alpha_r] d\alpha_r. \tag{7}$$

The integral is zero except for the discrete angles α_r of the array elements at values

$$\alpha_{ri} = \alpha_e + i(2\pi/M), \qquad 0 \le i \le M - 1. \tag{8}$$

At the i-th point, the integral has the solution

$$\int_{0}^{2\pi} \delta \left\{ \frac{2}{M} \sin \left[\frac{M}{2} (\alpha_{r} - \alpha_{e}) \right] \right\} \cos \left[\frac{M}{2} (\alpha_{r} - \alpha_{e}) \right]$$

$$\times \exp[j(q - l)\alpha_{r}] d\alpha_{r} = \exp[j(q - l)\alpha_{r}], \qquad (9)$$
399

and we can write

$$\overline{C}_{ql} = (\overline{C}_q/2\pi) \exp[j(q-l)\alpha_e]$$

$$\times \sum_{i=0}^{M-1} \exp[ji(q-l)2\pi/M]. \tag{10}$$

The sum on i in Eq. (10), abbreviated S_M , can be expressed in closed form [17] as

$$S_{M} = \frac{1 - \exp[j(q - l)2\pi]}{1 - \exp[j(q - l)2\pi/M]}.$$
 (11)

Since q - l is an integer, S_M is zero except when q - l = rM, with r an integer, Then, by l'Hospital's rule,

$$S_{M} = \begin{cases} M, q - l = rM \\ 0, q - l \neq rM \end{cases}$$
 (12)

Now Eq. (10) becomes, with Eq. (12),

$$\overline{C}_{ql} = \begin{cases} \frac{M\overline{C}_q}{2\pi} \exp[j(q-l)\alpha_e], & l = q - rM \\ 0, & l \neq q - rM \end{cases}$$
(13)

and the array excitation function Eq. (5) of a sampled mode can be expressed in terms of the original mode and a series of aliasing modes

$$\begin{split} \overline{E}_{qs} &= \frac{M\overline{C}_q}{2\pi} \exp[jq\alpha_e] \\ &\times \sum_{l=-\infty}^{\infty} \exp[jl(\alpha_r - \alpha_e)], \qquad l = q - rM. \end{split} \tag{14}$$

Thus the aliasing mode spectral responses are spaced at distances M with respect to q. Equation (14) can also be written as a summation over r and substituted into Eq. (3), so that the mode spectrum of the array excitation function becomes

$$\overline{E}_{s} = \frac{M}{2\pi} \sum_{q=-\infty}^{\infty} \overline{C}_{q} \exp[jq\alpha_{r}]$$

$$\times \sum_{q=-\infty}^{\infty} \exp[-jrM(\alpha_{r} - \alpha_{e})]. \tag{15}$$

Comparison of Eq. (15) with Eq. (3) shows that factor

$$\frac{M}{2\pi} \sum_{r=-\infty}^{\infty} \exp[-jrM(\alpha_r - \alpha_e)] = s(\alpha_r)$$

is the modal representation of the sampling function of Eq. (4).

Radiation coefficient of a mode

According to Eq. (15) the excitation function of a circular array can be expressed as a continuous ring excitation function consisting of an infinite number of modes due to the summation on r, even if the number of modes due to q is limited. Each mode of the excitation

function generates its counterpart in the radiation function in a one-to-one relationship. However, since the phase and amplitude relationship of these mode pairs is a function of the spatial frequency and the diameter of the array, we can say that the circular radiator acts as a linear filter on the spatial frequency spectrum of the excitation function to produce the spatial frequency spectrum of the radiation pattern. The transfer function of this filter is the radiation coefficient \bar{f}_a of a mode.

We assume that a differential element of a ring of radius R,

$$ds = Rd\alpha_{r} \tag{16}$$

exhibits a directional pattern $g(\theta, \epsilon)$, with

$$\theta = \alpha - \alpha_r,\tag{17}$$

which is assumed to be independent of the element location α_r on the circle, and can be expressed by a real function that is symmetric with respect to the radial plane $\theta=0$. Thus we can express the pattern in terms of a Fourier series

$$g(\theta, \epsilon) = \sum_{n=0}^{\infty} a_n(\epsilon) \cos n\theta.$$
 (18)

The contribution of the ring element to the ring radiation pattern due to the modal excitation $\overline{E}_q(\alpha_r)$ as defined in Eq. (3) is

$$d\overline{F}_{q} = \frac{c}{r(\alpha_{r})} \overline{C}_{q} \exp[jq\alpha_{r}] g(\theta, \epsilon)$$

$$\times \exp\left[-j\frac{r(\alpha_{r})}{\lambda} 2\pi\right] ds, \tag{19}$$

where

$$r(\alpha_r) = r_0 - R \cos \epsilon \cos (\alpha_r - \alpha), \tag{20}$$

Substituting Eqs. (16), (17), (18), and (20) into (19) yields the farfield pattern of the ring element

$$\begin{split} d\overline{F}_q &= \sigma \sum_{n=0}^{\infty} \overline{C}_q \, \exp[jq\alpha_r] a_n(\epsilon) \\ &\times \cos n\theta \, \exp[j\beta \cos \epsilon \, \cos \theta] d\alpha_r, \end{split} \tag{21}$$

where

$$\sigma = c \frac{R}{r_0} \text{ and } \beta = \frac{2\pi R}{\lambda}.$$
 (22)

Introducing θ as the sole variable, according to Eq. (17), leads to an integral form for the farfield pattern due to the entire ring excitation

$$F_{q} = \sigma \sum_{n=0}^{\infty} \overline{C}_{q} \exp[jq\alpha] a_{n}(\epsilon)$$

$$\times \int_{0}^{2\pi} \exp[-jq\theta] \cos n\theta \exp[j\beta \cos\epsilon \cos\theta] d\theta. \quad (23)$$

The integral in Eq. (23) can be split into two terms

$$I_{qn} = \frac{1}{2} \int_{0}^{2\pi} \exp[-j(q-n)\theta] \exp[j\beta \cos\epsilon \cos\theta] d\theta$$
$$+ \frac{1}{2} \int_{0}^{2\pi} \exp[-j(q+n)\theta] \exp[j\beta \cos\epsilon \cos\theta] d\theta. \tag{24}$$

for which the solutions are known [18],

$$I_{qn} = \pi j^{-(q-n)} J_{-(q-n)}(\beta \cos \epsilon)$$

+ $\pi j^{-(q+n)} J_{-(q+n)}(\beta \cos \epsilon).$ (25)

This expression can be transformed into [19]

$$I_{qn} = \pi j^q [j^{-n} J_{(q-n)}(\beta \cos \epsilon) + j^n J_{(q+n)}(\beta \cos \epsilon)]. \tag{26}$$

Since $j^q = \exp[q\pi/2]$ and $j^{\pm n} = \exp[\pm n\pi/2]$ Eq. (23) becomes

$$\overline{F}_{q} = \sigma \pi \sum_{n=0}^{\infty} \overline{C}_{q} \exp[jq(\alpha + \pi/2)]$$

$$\times a_{n}(\epsilon) \{ \exp[-jn\pi/2] J_{(q-n)}(\beta \cos \epsilon) + \exp[jn\pi/2] J_{(q-n)}(\beta \cos \epsilon) \}. \tag{27}$$

Eq. (27) constitutes a mode of the farfield pattern

$$\overline{F}_q = \overline{D}_q \exp[jq\alpha], \tag{28}$$

with

$$\begin{split} \overline{D}_{q} &= \pi \sigma \overline{C}_{q} \, \exp[jq\pi/2] \, \sum_{n=0}^{\infty} \, a_{n}(\epsilon) \\ &\quad \times \{ \exp[-jn\pi/2] J_{q-n}(\beta \, \cos \, \epsilon) \\ &\quad + \exp[jn\pi/2] J_{q+n}(\beta \, \cos \, \epsilon) \}, \end{split} \tag{29} \end{split}$$

the magnitude of the pattern mode. Thus the radiation coefficient of a mode is defined as

$$\overline{f_q} = \frac{\overline{F_q}}{\overline{E_q}} = \frac{\overline{D_q}}{\overline{C_q}} = \pi \sigma \exp[jq\pi/2] \sum_{n=0}^{\infty} a_n(\epsilon)
\times \{ \exp[-jn\pi/2] J_{q-n}(\beta \cos \epsilon)
+ \exp[jn\pi/2] J_{q+n}(\beta \cos \epsilon) \}.$$
(30)

It is interesting to note that the phase of the radiated mode changes with q in steps of $\pi/2$ with respect to the excited mode. A higher elevation ϵ effects the magnitude of the radiated mode in the same way as β , which means a reduced R/λ . Furthermore, since Bessel functions decay rapidly as the order increases beyond the magnitude of the argument, the spatial mode filter is a low-pass filter.

Two examples of greater interest to sonar engineering will give further insight into the characteristics of the mode radiation. The first example assumes omnidirectional ring elements, and the second assumes radiators with a cardioid pattern. Such patterns can be realized

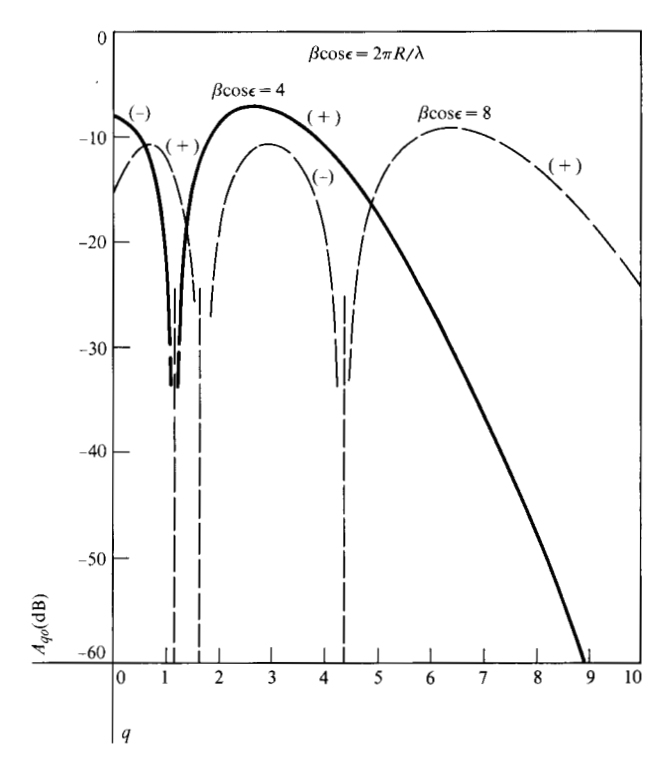


Figure 2 Mode radiation efficiency of a ring as determined by the circumference in terms of the wavelength or by the elevation angle of radiation. Point sources are omnidirectional.

by combining the outputs of a closely spaced pair of omnidirectional elements in a suitable network.

For the omnidirectional ring elements we set

$$g_0(\theta) = 1. (31)$$

Thus n = 0, $a(\epsilon) = a_0 = 1$ and

$$\overline{f_{q0}} = 2\pi\sigma \exp[jq\pi/2]J_q(\beta\cos\epsilon). \tag{32}$$

The logarithmic measure of the normalized power ratio becomes

$$A_{q0} = 10 \log \left(\frac{\bar{f}_{q0}}{2\pi\sigma}\right)^2 = 20 \log |J_q(\beta \cos \epsilon)|.$$
 (33)

A plot of the power ratio is illustrated in Fig. 2 for two values of the argument β cos ϵ . Therefore, the two curves can be interpreted in various ways. For example, for radiation in the ring plane with $\epsilon=0$, the curves relate to circumferences of four and eight wavelengths, or for a fixed normalized circumference of $\beta=8$, the curves relate to elevation angles of 0 and 60 degrees. The curves are plotted for $q \geq 0$; however, they also apply to q < 0 for integral values of q.

The curves show that the radiation coefficient drops off sharply, starting at $q = \beta \cos \epsilon$. There are also $(\beta/\pi) \cos \epsilon$ zeros of the Bessel function, which result in stop bands within the low-pass region. It may also be pointed

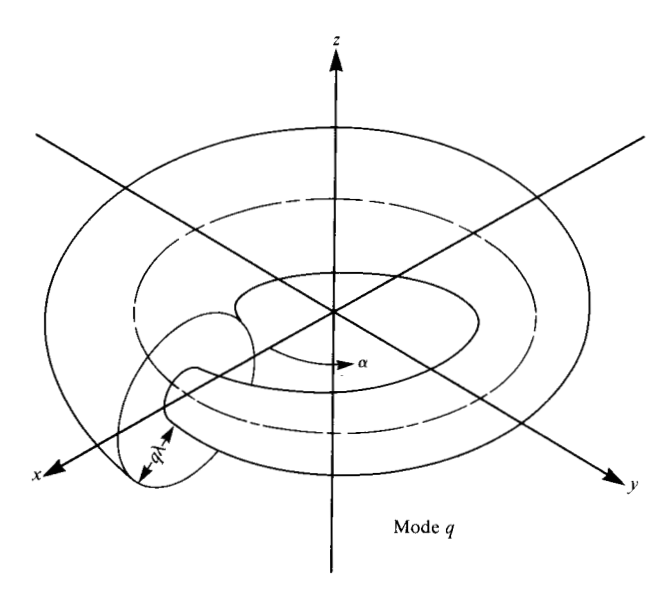


Figure 3 The excitation function of a mode of a circular radiator.

out that only the zero-order mode can radiate in the direction $\epsilon=90$ degrees. The illustration of the wavefront of a mode in Fig. 3 may help to show the physical characteristics of a modal radiation. It explains that the field contributions in the z direction cancel, even in the nearfield. It also shows that within the plane of the ring two spiral wavefronts radiate, one radiates away from the ring, and the other radiates toward the center. The latter will emerge from the center and interfere with the former spiral wave front. This results in the variations of the radiation coefficient within the passband.

For the cardioid directivity of the ring elements we set

$$g_c(\theta) = \frac{1}{2}(1 + \cos \epsilon \cos \theta). \tag{34}$$

Thus n = 0, 1; $a_0 = \frac{1}{2}$, $a_1 = \frac{1}{2} \cos \epsilon$ and

$$\overline{f}_{ac} = \pi \sigma \exp[jq\pi/2]$$

$$\times \, \{ J_q(\beta \, \cos \, \epsilon) \, + j \, \frac{\cos \, \epsilon}{2} \, [\, J_{q+1}(\beta \, \cos \, \epsilon) \,$$

$$-J_{a-1}(\beta\cos\epsilon)]\}. \tag{35}$$

The logarithmic measure of the normalized power ratio becomes

$$A_{qc} = 10 \log \left(\frac{\overline{f}_{qc}}{2\pi\sigma}\right)^{2}$$

$$= 10 \log \left\{ \frac{1}{4} [J_{q}(\beta \cos \epsilon)]^{2} + \frac{\cos^{2} \epsilon}{16} \right\}$$

$$\times [J_{q+1}(\beta \cos \epsilon) - J_{q-1}(\beta \cos \epsilon)]^{2}. \tag{36}$$

A plot of Eq. (36) is shown in Fig. 4 for the same two parameters as are used for the omnidirectional elements,

but the curves apply only to the plane of the ring, $\epsilon=0$. Since the spiral wave propagating toward the center no longer exists, the radiation coefficient does not show the variations caused by the interference of the two spiral waves of the omnidirectional case. The spatial frequency bandwidth, however, is not affected by the cardioid pattern.

It may be pointed out that baffled circular arrays can be treated with good approximation as arrays of elements with cardioid patterns, provided that the distance between the element and the baffle is small in terms of the diameter of the array [11].

Pattern synthesis from spatial frequency components and array design constraints

To determine the excitation function \overline{E} for a given beam pattern \overline{F} we first develop the pattern in a Fourier series [20]

$$\overline{F} = \sum_{q=-\infty}^{\infty} \overline{D}_q \exp[jq\alpha], \tag{37}$$

where

$$\overline{D}_{q} = \frac{1}{2\pi} \int_{0}^{2\pi} \overline{F} \exp[-jq\alpha] d\alpha.$$
 (38)

Then the spatial frequency components of the excitation function are computed according to Eq. (30),

$$\overline{C}_{a} = \overline{D}_{a} / \overline{f}_{a}. \tag{39}$$

Finally, the excitation function is computed. For the ring radiator we obtain the continuous function

$$\overline{E} = \sum_{q=-\infty}^{\infty} \overline{C}_q \exp[jq\alpha_r], \tag{40}$$

where

$$\overline{C}_{q} = \frac{1}{2\pi} \int_{0}^{2\pi} \overline{E} \exp[-jq\alpha_{r}] d\alpha_{r}. \tag{41}$$

The relation of Eq. (40) would, in theory, enable us to generate faithfully any pattern for which Eq. (38) has a solution. The sampling process by the array elements, however, results in the excitation function of Eq. (15), which leads to a pattern that deviates more or less from the desired beam shape, depending on the number M of elements.

A point source in the farfield generates the cophasal excitation function $E_{\rm c}$ with mode coefficients $C_{\rm qc}$. Hence multiplication by f_q would result in the mode coefficients $D_{\rm qc}$ of the cophasal beam pattern $F_{\rm c}$. To generate a different pattern F with mode coefficients D_q and C_q for the pattern and excitation functions, respectively, a transfer coefficient

$$\overline{t}_q = \overline{C}_q / \overline{C}_{qc} \tag{42}$$

must be included with the transmission coefficient $\overline{f_q}$ so that with Eq. (39)

$$\overline{D}_{q} = \overline{f}_{q} \overline{t}_{q} \overline{C}_{qc}. \tag{43}$$

Theoretically, there is no lower limit to the physical size of the array. However, significant higher modes of the pattern will fall into the region $|q| > \beta \cos \epsilon$, requiring a very high and precisely adjusted transfer coefficient \bar{t}_q . This region constitutes the supergain operation of the array [21]. While the supergain has been avoided by the designer of electromagnetic arrays because of the noise limitation in the receiver, a certain degree of supergain can be utilized in sonar arrays which operate with high background noise. Thus an intelligent tradeoff study is required to arrive at the optimum compromise of pattern directivity and physical array dimension.

After the size of the array has been decided, the number of elements must be determined. As shown, the elements sample the continuous excitation function \overline{E} and the sampled function $\overline{E}_{\rm s}$ with its aliasing spectrum of spatial frequencies is radiated. While the higher frequency components are severely attenuated by the low-pass filter action of the radiation process, we need be concerned only with the effect of the adjacent pair of aliasing modes. Thus for the computation of the array pattern the truncated form

$$E_{st} = \frac{M}{2\pi} \sum_{q=-q_{\rm m}}^{q_{\rm m}} \overline{C}_q \exp[jq\alpha_r]$$

$$\times \sum_{r=-1}^{+1} \exp[-jrM(\alpha_r - \alpha_e)], \tag{44}$$

may be substituted for Eq. (15), whereby q_m is chosen, where the modes make no relevant contribution to the pattern. To determine M we select the most demanding case of the highest desired mode q_h . Then the diameter of the array would be chosen

$$q_h \ge \beta$$
, with $\epsilon = 0$, (45)

depending whether supergain operation is required or not. Then the mode with r=-1 would be of no concern, but for r=1 the mode should be suppressed, i.e.,

$$q_h - M < -q_h$$

or, with Eq. (45),

$$M > 2q_b \ge 2\beta. \tag{46}$$

If, for example, an array of elements with cardioid pattern should be designed to radiate a pattern that ranges up to the eighth mode without operating in the supergain region, a normalized ring circumference of $\beta=8$ as illustrated in Fig. 4 would be the proper choice. To suppress the closest aliasing mode q_h-M by 10 dB we determine from the diagram $q_h-M=-10$, or M=18. Then

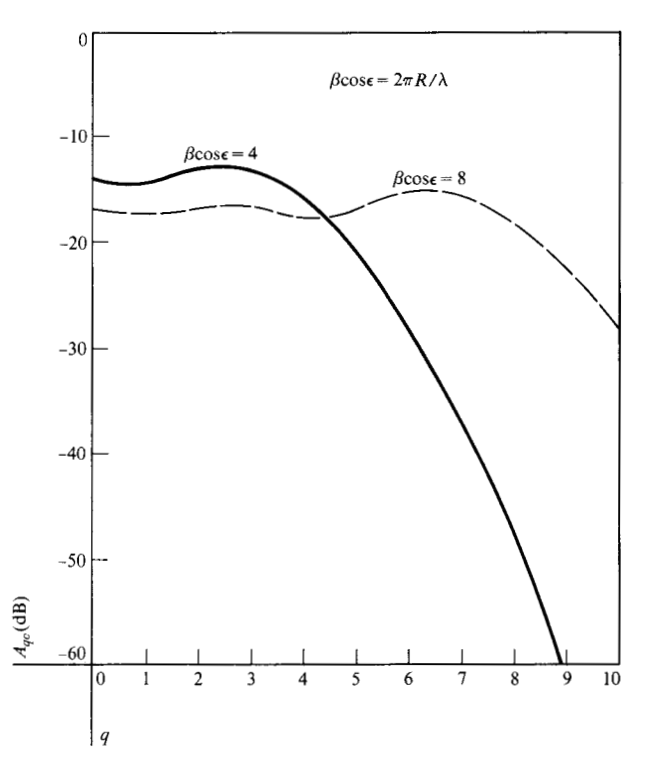


Figure 4 Mode radiation efficiency of a ring. The point sources, unlike those in Figure 2, have a cardioid pattern pointing radially outward.

the element spacing on the circumference β/M becomes 0.445 λ . This agrees with the experience of circular array designers that the element spacing should be less than $\lambda/2$ [22, 23]. For supergain designs, the number of elements increases with no theoretical limit.

Of course, the introduction of the FFT to the beamforming process will impose a similar constraint as with the Butler matrix. In both cases the number of array elements should be $M = 2^{\gamma}$, with γ an integer.

It may be pointed out that multiplication of \overline{C}_q by $\exp[jq\alpha]$ rotates each mode of the excitation function and hence the pattern by the azimuth angle α . This simple process is another useful feature of the pattern synthesis from excitation function modes.

The beamforming network and its theory

The digital processing of broadband signals for fast beamforming with circular arrays consists of the following steps:

- 1. Spectral resolution of the received signals by means of the Fast Fourier Transform.
- 2. Modal resolution of the spectral bands by means of fast mode formers (FMFs).
- Weighting of the mode outputs by complex multiplications.

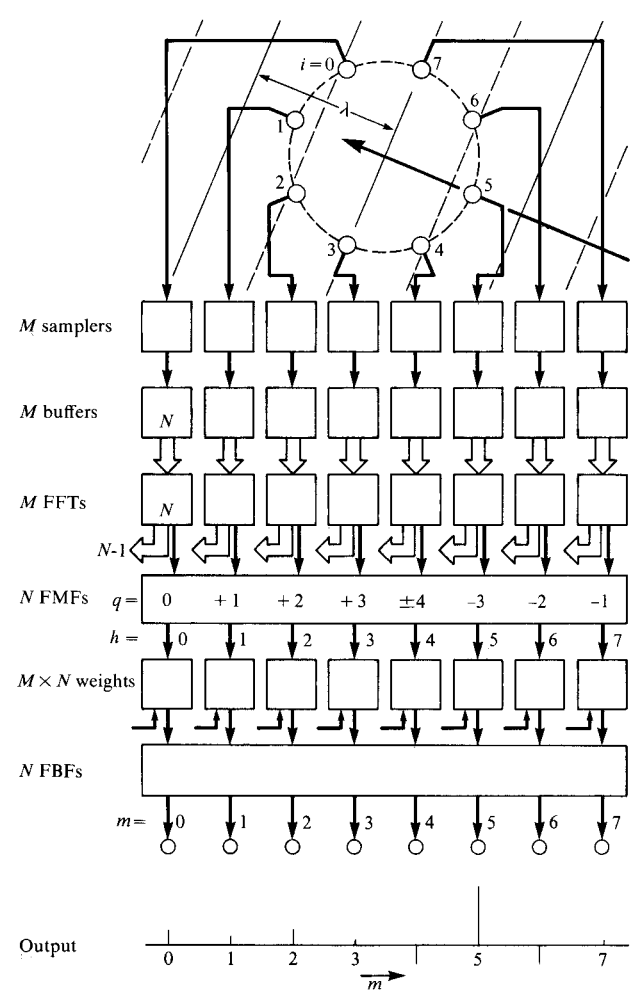


Figure 5 Block diagram of the fast beamformer for a circular array.

4. Pattern synthesis by processing the weighted mode outputs in fast beam formers (FBFs).

The block diagram of Fig. 5 illustrates how these four steps are carried out. The array consists of M = 8 elements counted in i. Radiation is assumed from a distant source in the direction of element 5. A bank of M samplers samples the broadband signal at a rate commensurate with the requirements for the highest frequency. Batches of N samples are stored in a bank of buffers and transferred to a bank of M FFTs, which deliver N samples of the spectral distribution. Samples of the same spectral band originating from all the elements are fed through N FMFs. Each FMF delivers M mode outputs identified by q, and the terminals are counted in h. Each mode sample is weighted, requiring a total of $M \cdot N$ weights. The multipliers are derived externally so that beam shapes can be controlled. Finally, the weighted mode samples are fed through N FBFs which generate M samples of the angular distribution of radiation.

The number $N=2^{\gamma}$ equally spaced time samples x(k) of the signal x(t) determines the spectral resolution which must be adequate to enable the identification of modes that depend on the phasor concept. However, in most cases the objective of signal identification requires a much higher resolution than the beamformer. The FFT delivers N equally spaced samples s(n) of the frequency spectrum s(f) according to the algorithm [24]

$$s(n) = \frac{1}{N} \sum_{k=0}^{N-1} x(k) \exp[-j2\pi nk/N], \tag{47}$$

with

$$x(k) = \sum_{n=0}^{N-1} s(n) \exp[j2\pi nk/N].$$
 (48)

Frequency and time spacings Δf and Δt , respectively, are related by

$$\Delta f = 1/N\Delta t,\tag{49}$$

so that the time samples of a signal of frequency f, received by element i, take the form

$$x(k) = x_0 \cos \left(2\pi f k \Delta t + \psi_i + \phi_0\right), \tag{50}$$

or

$$x(k) = \frac{x_0}{2} \left\{ \exp[j(2\pi f k \Delta t + \psi_i + \phi_0)] + \exp[-j(2\pi f k \Delta t + \psi_i + \phi_0)]. \right\}$$
(51)

Then the spectral samples become, according to Eq. (47),

$$s(n) = \frac{1}{N} \sum_{k=0}^{N-1} \frac{x_0}{2} \left(\exp\{j[2\pi k (f\Delta t - n/N) + \psi_i + \phi_0]\} + \exp[-j(2\pi k (f\Delta t + n/N) + \psi_i + \phi_0)] \right).$$
 (52)

The summations can be expressed by single terms [17]

$$s(n) = \frac{x_0}{2} \left(\frac{\sin \left[(fT - n)\pi \right]}{N \sin \left[\frac{1}{N} (fT - n)\pi \right]} \right)$$

$$\times \exp \left\{ j \left[\frac{N - 1}{N} (fT - n)\pi + \psi_i + \phi_0 \right] \right\}$$

$$+ \frac{\sin \left[(fT + n)\pi \right]}{N \sin \left[\frac{1}{N} (fT + n)\pi \right]}$$

$$\times \exp \left\{ -j \left[\frac{N - 1}{N} (fT + n)\pi + \psi_i + \phi_0 \right] \right\} \right). (53)$$

This equation reveals two responses with the envelopes

$$\frac{\sin\left[(fT\mp n)\pi\right]}{N\sin\left[\frac{1}{N}\left(fT\mp n\right)\pi\right]} = S_n^{\mp}$$
 (54)

and the phases

$$\frac{N-1}{N} (fT \mp n)\pi + \psi_i + \phi_0 = \sigma^{\mp} + \psi_i + \phi_0.$$
 (55)

The envelopes peak at

$$fT \mp n = 0, \pm N, \pm 2N \cdots, \tag{56}$$

where the solution n=fT refers to the desired response, while aliasing due to sampling causes the remaining responses. Also the side lobes of the envelopes cause undesired responses. Design conditions of FFTs are well established [24] to avoid aliasing by the choice of high sampling rates and minimize side lobe responses by nonuniform weighting of the samples. The important fact, however, should be noted that the phase of the signal of the elements ψ_i is preserved in the spectral samples. This phase results in a rather complex way from the superposition of the constituent modes of the array excitation function. To trace the effect of a mode through the FMF we set

$$\psi_i = 2\pi q \, \frac{i}{M} \tag{57}$$

and simplify the spectral expression by substituting Eqs. (54) and (55) into Eq. (53). Thus

$$s(n, i) = \frac{x_0}{2} \left\{ S_n^- \exp[j(\sigma_n^- + 2\pi q i/M + \phi_0)] + S_n^+ \exp[-j(\sigma_n^+ + 2\pi q i/M + \phi_0)] \right\}.$$
 (58)

Applying the same algorithm to the spectral sample processing in the FMF as shown for the time function samples to generate the spectral samples, we obtain

$$u(n, h) = \frac{x_0}{2} \{ S_n^- U_h^- \exp[j(\sigma_n^- + \mu_h^- + \phi_0) + S_n^+ U_h^+ \exp[-j(\sigma_n^+ + \mu_h^+ + \phi_0)] \}, (59)$$

where
$$0 \le h \le M - 1$$
, (60)

$$U_h^{\mp} = \frac{\sin\left[(q \mp h)\pi\right]}{M\sin\left[\frac{1}{M}(q \mp h)\pi\right]},\tag{61}$$

and
$$\mu_h^{\mp} = \frac{M-1}{M} (q \mp h)\pi$$
. (62)

With proper design the second term in Eq. (58) is insignificant. Therefore the mode response develops peaks only due to the envelope U_h^- at

$$h - q = 0, \pm M, \pm 2M, \cdots \tag{63}$$

Since the sampling theorem requires that |q| < M/2, the mode responses appear at the terminals as defined by the solutions

$$q > 0,$$
 $h - q = 0,$ $q < 0,$ $h - q = M.$ (64)

To generate the beam response we must compensate for the radiation coefficient of the modes and adjust the modes to the spatial frequency spectrum of the desired pattern by weighting each mode by the factor

$$\overline{\mathbf{W}}_{h} = w_{h} \exp[j\nu_{h}] = \overline{f}_{a}\overline{t}_{a} \tag{65}$$

as derived in Eqs. (30) and (42). Since $\bar{f}_q = \bar{f}_{-q}$ and $\bar{t}_q = \bar{t}_{-q}$, only M/2 different weights are required for each beamformer. The weighted mode responses can then be expressed by

$$v(n, h) = \frac{x_0}{2} \left\{ S_n^- V_h^- \exp[j(\sigma_n^- + \mu_h^- + \nu_h^- + \phi_0^-)] + S_n^+ V_h^+ \exp[-j(\sigma_n^+ + \mu_h^+ + \nu_h^- + \phi_0^-)] \right\}$$
(66)

with

$$\mathbf{V}_{h}^{\ \tau} = w_{h} \mathbf{U}_{h}^{\ \tau}. \tag{67}$$

In the final stage of the beamforming network the weighted mode responses are added to form the pattern. As discussed above, the phase shifting of the modes by $\exp[jq\alpha]$ means a rotation of the modes and hence of the pattern by the azimuth angle α . An inverse FFT performs the process of phase shifting and adding according to the algorithm stated in Eq. (48). Thus an FBF performs the computation

$$b(n, m) = \sum_{h=0}^{M-1} v(n, h) \exp[-j2\pi mh/M]$$
 (68)

and yields as many beam responses as array elements, uniformly distributed over the azimuth. Since the beams are about as wide as their separations, good azimuth coverage can be achieved. With background and single source radiation distributed over the azimuth, the FBF provides a sampled panoramic display. Substituting Eq. (66) into Eq. (68) yields

$$b(n, m) = \frac{x_0}{2} \left\{ S_n^- V_n^- \exp[j(\sigma_n^- + \phi_0)] \right.$$

$$\times \sum_{h=0}^{M-1} \exp[j(\mu_h^- + \nu_h - 2\pi mh/M)]$$

$$+ S_n^+ V_n^+ \exp[-j(\sigma_n^+ + \phi_0)]$$

$$\times \sum_{h=0}^{M-1} \exp[-j(\mu_h^+ + \nu_h + 2\pi mh/M)] \right\}. (69)$$

Cophasal beam excitation and pattern of a circular array

An example of general interest is the cophasal excitation of the circular array to generate a beam in the direction α_b , ϵ_b [12]. The field strength contribution of an omnidirectionally radiating ring element is

$$d\overline{F} = \frac{c}{r(\alpha_1)} \overline{E}(\alpha_r) \exp\left[-j\frac{r(\alpha_r)}{\lambda} 2\pi\right] ds. \tag{70}$$

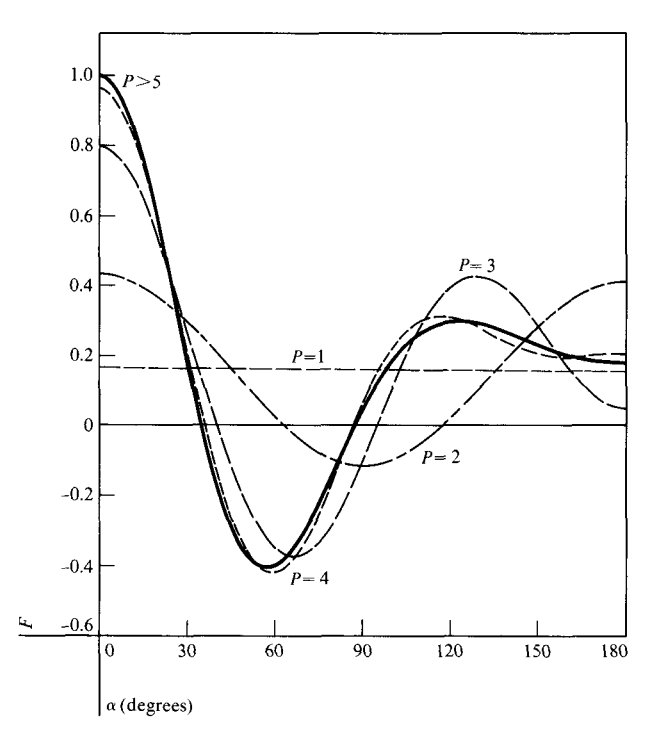


Figure 6 Patterns of a cophasally excited circular radiator of four wavelengths circumference if the mode spectrum is limited to $P = p_{\rm max}$ as indicated.

Substituting Eqs. (20) and (22) into Eq. (70) yields, under the farfield condition,

$$d\overline{F} = \sigma \overline{E}(\alpha_r) \exp[j\beta \cos \epsilon \cos(\alpha_r - \alpha)] d\alpha_r. \tag{71}$$

The expression for $\overline{E}(\alpha_r)$ can readily be derived from Eq. (71), since all ring elements must be phased so that their contributions in the direction α_b and ϵ_b add up cophasally. Thus

$$\overline{E}(\alpha_r) = E_{\rho} \exp[-j\beta \cos \epsilon_{\rm b} \cos (\alpha_r - \alpha_{\rm b})]. \tag{72}$$

Substituting Eq. (72) into Eq. (71) results in

$$d\overline{F} = \sigma E_{c} \exp\{j\beta[\cos\epsilon\cos(\alpha_{r} - \alpha) - \cos\epsilon_{b}\cos(\alpha_{r} - \alpha_{b})]\}d\alpha_{r}. \tag{73}$$

Applying trigonometric identities, we derive

$$d\overline{F} = \sigma E_c \exp[j\beta g \sin((\alpha_r + \gamma))] d\alpha_r$$

where

$$g = [\cos^2 \epsilon + \cos^2 \epsilon_b - 2 \cos \epsilon \cos \epsilon_b \cos (\alpha - \alpha_b)]^{\frac{1}{2}}$$

and

$$\gamma = \arctan \frac{\cos \epsilon \cos \alpha - \cos \epsilon_b \cos \alpha_b}{\cos \epsilon \sin \alpha - \cos \epsilon_b \sin \alpha_b}, \tag{74}$$

then

$$\overline{F} = \sigma E_c \int_0^{2\pi} \exp[j\beta g \sin(\alpha_r + \gamma)] d\alpha_r. \tag{75}$$

Integration yields the real function [18]

$$F = 2\pi\sigma E_c J_o(\beta g). \tag{76}$$

With the beam pointed in the direction $\alpha_b = \epsilon_b = 0$, the azimuth pattern becomes

$$F_{0a} = 2\pi\sigma E_{c} J_{0} \left(2\beta \sin \frac{\alpha}{2} \right). \tag{77}$$

The normalized form of Eq. (77),

$$F_{0an} = J_0 \left(2\beta \sin \frac{\alpha}{2} \right), \tag{78}$$

is plotted by a solid line in Fig. 6. It constitutes the limiting case of an array with $M \rightarrow \infty$ elements.

To express the cophasal beam pattern in terms of its modes, we first derive the modal form of the excitation function Eq. (72). According to Eq. (41), the mode coefficients are

$$\overline{C}_{q} = \frac{E_{c}}{2\pi} \int_{0}^{2\pi} \exp[-jq\alpha_{r}]$$

$$\times \exp[-j\beta \cos \epsilon_{b} \cos (\alpha_{r} - \alpha_{b})] d\alpha_{r}. \tag{79}$$

Solution of the integral yields [18]

$$\overline{C}_q = E_c \exp[-jq(\alpha_b + \pi/2)] J_q (\beta \cos \epsilon_b).$$
 (80)

Then, according to Eqs. (32), (37), and (39) with $\bar{t}_a = 1$,

$$\overline{F} = 2\pi\sigma E_c \sum_{q=-\infty}^{\infty} \times \exp[jq(\alpha - \alpha_b)] J_a(\beta \cos \epsilon_b) J_a(\beta \cos \epsilon).$$
 (81)

The equality of the expressions of Eq. (76) and (81) can be shown with the aid of Graf's formula [25]. The normalized pattern in the azimuth plane for a beam pointing in the direction $\alpha_b = \epsilon_b = 0$ can be expressed by

$$F = J_0^2(\beta) + 2 \sum_{p=1}^{\infty} J_p^2(\beta) \exp[jp\alpha], \qquad p = |q|,$$
 (82)

note that
$$J_{-q}^2(\beta) = J_q^2(\beta)$$
 when $q = \text{integer [18]}$.

Figure 6 also shows plots of patterns consisting of a limited number of modes. As explained by Fig. 2 the first order mode and the modes of order higher than β have almost negligible effects on the pattern development.

The conventional expression for the array pattern can readily be formulated by substituting the contribution \overline{F}_i of an element at the location $\alpha_i = \alpha_e + i2\pi/M$ for the contribution $d\overline{F}$ of a differential ring element in Eq. (73) and summing the contributions of all elements:

$$\overline{F} = \sigma E_{c} \sum_{i=0}^{M-1} \exp \left\{ j\beta \left[\cos \epsilon \right] \right.$$

$$\times \cos \left(i \frac{2\pi}{M} + \alpha_{e} - \alpha \right) - \cos \epsilon_{b}$$

$$\times \cos \left(i \frac{2\pi}{M} + \alpha_{e} - \alpha_{b} \right) \right] \right\}.$$
(83)

Hence the normalized azimuth pattern of a beam pointing in the direction of element i = 0 at $\alpha_e = 0$ becomes

$$\overline{F} = \frac{1}{M} \sum_{i=0}^{M-1} \exp \left\{ j\beta \left[\cos \left(i \frac{2\pi}{M} - \alpha \right) - \cos i \frac{2\pi}{M} \right] \right\}. \tag{84}$$

The pattern of Eq. (84) has been plotted in Fig. 7.

To express the array pattern in terms of its modes, we first substitute the mode coefficients of the excitation function of Eq. (80) into Eq. (15) to obtain the excitation function

$$\overline{E_s} = \frac{ME_c}{2\pi} \sum_{q=-\infty}^{\infty} \exp[jq(\alpha_r - \alpha_b - \pi/2)]$$

$$\times J_q(\beta \cos \epsilon_b) \sum_{r=-\infty}^{\infty} \exp[-jrM(\alpha_r - \alpha_e)].$$
 (85)

which indicates a mode spectrum of orders q - rM. Then the pattern is obtained by multiplying the excitation function modes with the respective radiation coefficients as derived in Eq. (32)

$$\begin{split} \overline{F_s} &= \sigma M E_{\rm c} \sum_{q=-\infty}^{\infty} \exp[jq(\alpha - \alpha_{\rm b})] \\ &\times J_q(\beta \cos \epsilon_{\rm b}) \sum_{r=-\infty}^{\infty} \exp[-jrM(\alpha - \alpha_{\rm e} + \pi/2)] \\ &\times J_{(q-rM)}(\beta \cos \epsilon). \end{split} \tag{86}$$

Of course, the summations of Eq. (85) and (86) can be truncated as discussed with Eq. (44). For the azimuth pattern of a beam, aligned with $\alpha_{\rm b}=\epsilon_{\rm b}=0$, the truncated normalized form becomes

$$\overline{F}_{stn} = \sum_{q=-q_m}^{q_m} \exp[jq\alpha] J_q(\beta)$$

$$\times \sum_{r=-1}^{1} \exp[-jrM(\alpha + \pi 2)] J_{(q-rM)}(\beta). \tag{87}$$

Computer simulation of the fast beamforming process

To check out the fast beamforming process, a computer simulation was performed using an APL program. A single frequency signal was assumed so that the FFTs yielded the array element signals as derived from Eq. (72) in the normalized form

$$s(i) = \exp\left[j\beta \cos \epsilon_{\rm b} \cos\left(i\frac{2\pi}{M} + \alpha_{\rm e} - \alpha_{\rm b}\right)\right]. \tag{88}$$

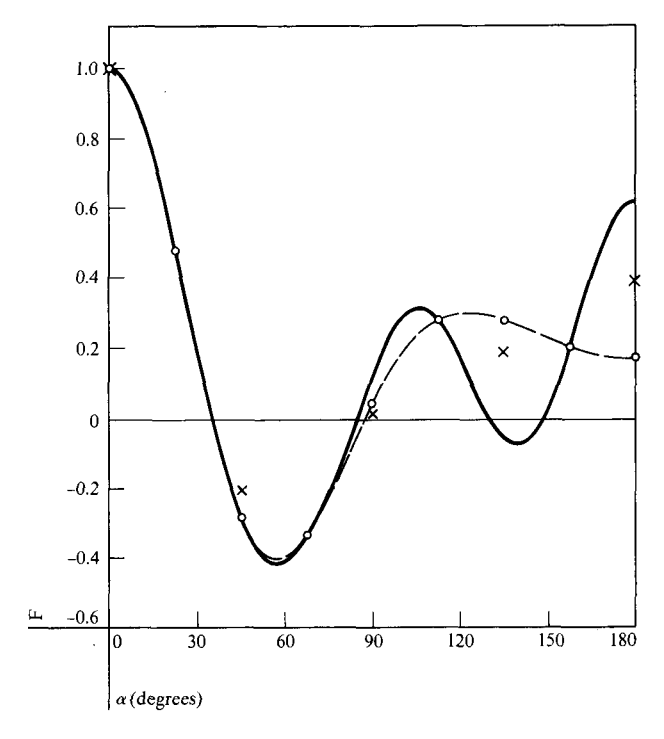


Figure 7 Patterns of a cophasally excited circular array of four wavelengths circumference. With eight elements the pattern takes the shape of the solid line and fast beamformer (FBF) responses are defined by the × points. The dashed line and "o" points refer to the pattern and FBF responses for 16 elements.

The M complex terms of Eq. (88) were separated into their real and imaginary components, which constitute a $2 \times M$ matrix. Then the matrix terms were transformed by the FFT routine to yield a $2 \times M$ matrix of mode terms u(h).

The weights of the mode terms were derived from Eq. (32) according to Eq. (65) with $\bar{t}_q = 1$. The ambiguities due to sampling will cause all modes $q \pm rM$ to respond at the terminal h = q. With properly designed arrays only modes |q| < M/2 are significant. Therefore modes and terminals are related as follows:

$$q = h, q < M/2$$

$$q = h - M, q \ge M/2.$$
(89)

The normalized weights thus become

$$\overline{W}_h = \exp[jh\pi/2]J_h(\beta\cos\epsilon), \qquad 0 \le h < M/2$$

$$\overline{W}_h = \exp[j(h-M)\pi/2]J_{h-M}(\beta\cos\epsilon), \qquad M/2 \le h < M$$
(90)

Now the complex multiplication of the weights and the mode terms is performed.

In the final computation the inverse FFT routine is applied to the weighted modes and yields the beam pattern samples for cophasal excitation.

To enable comparison with previous plots, the example of an array with $\beta=4$ and M=8 was chosen and the responses of the fast beamformer plotted in Fig. 7 as "×" marks together with the theoretical pattern according to Eq. (84) shown by a solid line. The deviation in the back lobe sector is not unexpected, because according to Figs. 2 and 6 the modes of order ± 4 contribute significantly to the cophasal beam pattern and can not be defined by eight elements according to the sampling theorem. Doubling the number of elements not only results in excellent agreement of the fast beamformer responses with the theoretical pattern, as indicated by the "o" marks and the dashed line, it also results in excellent agreement of the array pattern with that of the ring as plotted in Fig. 6.

From the above example, it can be concluded that the limitation to correctly sample a given pattern by the FBF technique lies solely in the density of array elements. If the elements cannot adequately sample the required excitation function, the pattern will be incorrectly represented. This limitation applies to the conventional beamforming technique as well, although the pattern deviates from the given pattern in a different way.

Note added in proof

While this paper was in proof, two additional references [26, 27] came to the attention of the author.

Acknowledgments

The author is indebted to Stuart F. Adams for his suggestion to study a more efficient digital beam forming technique for circular arrays and to Gordon L. DeMuth for the helpful discussions during the progress of this study.

References

- I. D. Longstaff, P. E. K. Chow, and D. E. N. Davies, "Directional Properties of Circular Arrays", *Proc. IEEE* 114, 713 (1967).
- J. E. Boyns, C. W. Gorham, A. David Munger, Joseph H. Provencher, J. Reindel, and B. I. Small, "Step-Scanned Circular-Array Antenna", *IEEE Trans. Antennas and Propagation* AP-18, 590 (1970).
- J. D. Tillman, W. T. Patton, C. E. Blakely and F. V. Schultz, "The Use of a Ring Array as a Skip Range Antenna," Proc. IRE 43, Part I, 1655 (1955).
- W. Burkhardtsmaier and U. Finkbein, "Kreisgruppenantennen als Rund- und Richtstrahler," *Elektrotechnik* (Berlin) 4, 239 (1950).
- D. E. N. Davies and B. S. McCartney, "Cylindrical Arrays with Electronic Beam Scanning," Proc. IEE 112, 497 (1965).
- J. Butler and R. Lowe, "Beamforming Matrix Simplifies Design of Electronically Scanned Antennas," *Electronic Design* 9, 170 (April 12, 1961).

- 7. J. R. Williams, "Fast Beam-Forming Algorithm," J. Acoust. Soc. Amer. 44, 1454 (1968).
- 8. G. Sinclair, "The Patterns of Slotted-Cylinder Antennas," *Proc. IRE* 36, 1487 (1948).
- 9. B. S. McCartney, "Proposals for an Electronically Scanned Circular Array," *Proc. IEE* 110, 1220 (1963).
- R. G. Fenby and D. E. N. Davies, "Circular Array Providing Fast 360° Electronic Beam Rotation," Proc. IEE 115, 78 (1968).
- G. C. Chadwick and J. C. Glass, "Investigation of a Multiple Beam Scanning Circular Array," Scientific Report No. 1 to USAF, Cambridge Research Lab., Cambridge, MA, Contract AF19 (628) 367, Dec. 31, 1962.
- B. Sheleg, "A Matrix-Fed Circular Array for Continuous Scanning," Proc. IEEE 56, 2016 (1968).
- 13. W. R. LePage, C. S. Roys and S. Seely, "Radiation from Circular Current Sheets," *Proc. IRE* 38, 1069 (1950).
- R. F. Harrington and W. R. LePage, "Directional Antenna Arrays of Elements Circularly Disposed About a Cylindrical Reflector," Proc. IRE 40, 83 (1952).
- 15. H. L. Knudsen, "Radiation from Ring Quasi-Arrays," IRE Trans. Antennas and Propagation AP-4, 452 (1956).
- R. W. Redlich, "Sampling Synthesis of Ring Arrays," IEEE Trans. Antennas and Propagation AP-18, 116 (1970).
- W. Silver, Microwave Antenna Theory and Design, McGraw-Hill Book Company, Inc., New York, 1949, p. 264.
- 18. E. Jahnke and F. Emde, *Tables of Functions*, Dover Publications, New York, p. 149.
- 19. Ibid., p. 128.
- J. R. Wait and J. Householder, "Pattern Synthesis for Slotted-Cylinder Antennas," J. Res. Nat. Bur. Stand. 63-D, 303 (1959).
- W. W. Hansen and J. R. Woodyard, "A New Principle in Directional Antenna Design," Proc. IRE 26, 333 (1938).
- Ta-Shing Chu, "On the Use of Uniform Circular Arrays to Obtain Omnidirectional Patterns," IRE Trans. Antennas and Propagation AP-7, 436 (1959).
- N. Goto and D. K. Cheng, "On the Synthesis of Concentric-Ring Arrays," Proc. IEEE 117, 839 (1970).
- 24. G. D. Bergland, "A Guided Tour of the Fast Fourier Transform," *IEEE Spectrum* **6**, 41 (1969).
- G. N. Watson, A Treatise on the Theory of Bessel Functions, Cambridge University Press, New York, 2nd Edition, p. 360.
- 26. D. R. Farrier, T. S. Durrani, and J. M. Nightingale, "Fast Beamforming Techniques for Circular Arrays," *J. Acoust. Soc. Amer.* 58, 920 (1975).
 27. W. F. Gabriel, "Adaptive Arrays An Introduction," *Proc.*
- 27. W. F. Gabriel, "Adaptive Arrays An Introduction," *Proc IEEE* 64, 239 (1976).

Received April 25, 1974

The author, at the time this paper was written, was with the IBM Federal Systems Division, 18100 Frederick Pike, Gaithersburg, Maryland 20760. He is now retired from IBM.